IFAC Journal of Systems and Control 35 (2026) 100393

Contents lists available at ScienceDirect

IFAC Journal of Systems and Control

journal homepage: www.elsevier.com/locate/ifacsc

Full Length Article

# A robust tube-based MPC approach for safer insulin dosing☆,☆☆

Nicola Licini *, Marcelo Alves Santos, Fabio Previdi, Antonio Ferramosca

*Department of Management, Information and Production Engineering, University of Bergamo, 24044 Dalmine, Bergamo, Italy*

ARTICLE INFO

*Article history:*
Received 2 November 2025
Received in revised form 30 January 2026
Accepted 17 February 2026
Available online 23 February 2026

*Keywords:*
Robust model predictive control
Type 1 diabetes
Artificial pancreas

ABSTRACT

We present a robust model predictive control (MPC) approach for safer insulin dosing in artificial pancreas systems. The method applies estimation-informed constraint tightening to maintain safety under disturbances and unmodeled dynamics. Safety margins, derived from estimator confidence, are enforced as tube-based tightening on state and input constraints. A zone control objective targets a glucose band with asymmetric weights that emphasize avoidance of low glucose. Simulation studies show fewer low glucose events and lower violation risk than a nominal MPC baseline, with comparable dosing effort. The contribution of this work is a robust zone MPC scheme that maps estimator uncertainty into safety margins for insulin dosing.

© 2026 The Author(s). Published by Elsevier Ltd. This is an open access article under the CC BY license (http://creativecommons.org/licenses/by/4.0/).

## 1. Introduction

Type 1 diabetes (T1D) is a chronic autoimmune disorder characterized by the near-complete destruction of pancreatic $\beta$-cells, leading to a loss of endogenous insulin secretion. Consequently, individuals with T1D require lifelong exogenous insulin administration to maintain blood glucose (BG) within the clinically safe range of euglycemia (70–180 mg/dL). Sustained hyperglycemia (BG$>$180 mg/dL) contributes to long-term micro- and macrovascular complications, whereas hypoglycemia (BG$<$70 mg/dL) poses immediate, potentially life-threatening risk (Katsarou et al., 2017). Achieving tight yet safe glycemic control thus demands strategies that are both adaptive and robust to the significant variability encountered in daily life.

Closed-loop artificial pancreas (AP) systems integrate a continuous glucose monitor (CGM), an insulin pump, and a control algorithm to automate insulin delivery and reduce patient burden. Hybrid AP designs still depend on meal announcements and manual boluses to manage postprandial excursions, whereas fully closed-loop approaches aim to eliminate such manual inputs, thereby simplifying therapy and enhancing autonomy. Despite major progress in sensor accuracy, insulin delivery technology, and control design, achieving sustained, fully autonomous regulation remains an open challenge. Physiological and technological constraints introduce delays, uncertainties, and disturbances that act over multiple time scales, fundamentally limiting closed-loop performance (Reiterer et al., 2018). In practice, digestion dynamics and subcutaneous insulin absorption introduce substantial lags; CGM signals are affected by noise and calibration errors; and external factors such as unannounced meals, and/or inaccurately announced meals, exercise, stress, illness, and circadian modulation act as large, time-varying disturbances. Moreover, inter- and intra-patient variability, parameter drift, model mismatch, and sensor artifacts further complicate both prediction and feedback. These realities highlight the stringent need for control algorithms that explicitly account for uncertainty and constraints, ensuring protection against hypoglycemia without resorting to overly conservative insulin delivery that compromises glycemic regulation.

Model predictive control (MPC) has emerged as a compelling framework for the AP (Magni et al., 2007; Messori et al., 2018), as it naturally accommodates system dynamics, constraints, and future information through prediction. MPC can forecast BG trajectories, enforce safety-relevant limits on insulin infusion and glucose levels, and adapt to disturbances across multiple time scales. In particular, Zone MPC (ZMPC) formulations, which target a clinically meaningful glucose band rather than a fixed setpoint, align closely with therapeutic objectives. They allow asymmetric penalization to reflect the clinical asymmetry of risks, assigning stronger penalties to hypoglycemia than to mild hyperglycemia (Abuin et al., 2020).

Beyond nominal or zone-oriented formulations, tube-based robust MPC approaches address bounded disturbances and model mismatch by maintaining the true state within an invariant tube around a nominal trajectory and enforcing tightened constraints

☆ This article is part of a Special issue entitled: 'IFAC WC 2026 - TC 8.2' published in IFAC Journal of Systems and Control.

☆☆ This work was funded by the National Plan for NRRP Complementary Investments (PNC, established with the decree-law 6 May 2021, n. 59, converted by law n. 101 of 2021) in the call for the funding of research initiatives for technologies and innovative trajectories in the health and care sectors (Directorial Decree n. 931 of 06-06-2022) – project n. PNC0000003 – AdvaNced Technologies for Human-centrEd Medicine (ANTHEM).

* Corresponding author.
*E-mail address:* nicola.licini@unibg.it (N. Licini).

https://doi.org/10.1016/j.ifacsc.2026.100393
2468-6018/© 2026 The Author(s). Published by Elsevier Ltd. This is an open access article under the CC BY license (http://creativecommons.org/licenses/by/4.0/).

to achieve robust constraint satisfaction (Mayne et al., 2005). In fact, with standard ingredients, tube-based MPC ensures recursive feasibility and robust stability, while retaining computational tractability comparable to nominal MPC through precomputed constraint tightening.

Despite its strong theoretical appeal and widespread adoption in other safety-critical domains such as aerospace and process control (Ding et al., 2018; Mirshams & Khosrojerdi, 2016), tube-based MPC has received limited attention in the context of glucose regulation for T1D. Early work demonstrated the feasibility of tube-based robust MPC for glucose regulation in simulation (Kirchsteiger & del Re, 2013), while more recent contributions have investigated tube-based MPC formulations to enhance robustness under generic perturbations (Jia et al., 2024). Nevertheless, the integration of tube-based designs with AP-specific objectives, uncertainty sources, and evaluation protocols remains limited.

In contrast, robustness in existing adaptive MPC strategies for T1D is more commonly addressed through adaptive MPC strategies, such as adjusting control parameters based on meal anticipation (Colmegna et al., 2022), or through the use of ad hoc safety margins. While effective in practice, these approaches do not provide explicit set-based guarantees of constraint satisfaction under bounded uncertainty, as in tube-based MPC designs.

Motivated by these considerations, this work proposes a tube-based ZMPC formulation tailored to the AP control. The proposed controller systematically propagates uncertainty through prediction to enforce mathematically consistent constraint tightenings on both glucose and insulin trajectories. Consistently with hybrid AP operation, we assume that meal announcements are available to the controller, yet they may be substantially inaccurate (i.e., under-/over-estimated), and this mismatch is explicitly treated as a disturbance/uncertainty. It further incorporates (i) offset-free state estimation, and (ii) zone-based objectives that prioritize hypoglycemia avoidance while enabling efficient recovery from hyperglycemia. Through explicit uncertainty handling, rather than heuristic conservatism or user intervention, the proposed design aims to preserve safety and performance in the dynamic, unpredictable conditions of free-living T1D. Validation using the FDA-accepted UVA/Padova T1D simulator (Man et al., 2014) under misannounced meals scenarios demonstrates the effectiveness of the approach.

This paper is organized as follows. Section 2 introduces the model, estimator, and constraint sets. Section 3 presents the tube-based ZMPC with estimation-informed constraint tightening and offset-free. Section 4 details the simulation setup and results against a nominal MPC, including hypoglycemia metrics and dosing effort. Section 5 concludes the work.

## 2. Modeling, estimation, and constraints

This section presents the modeling and estimation framework used in the proposed approach. A discrete-time nonlinear system with partially known exogenous inputs is represented by a linear affine model augmented with a disturbance state to capture unmodeled effects and support offset-free estimation. The disturbance is decomposed into a deterministic term and an estimation-error term. Moreover, residual process and measurement noises are treated as random variables with Gaussian distributions, and a linear Kalman filter is used to estimate the state and the disturbance. The filter covariance is then converted into a deterministic uncertainty set at a chosen confidence level, which will later support constraint tightening procedures.

### 2.1. Modeling

Consider the following discrete-time nonlinear system representing the discretization of the underlying continuous-time system, i.e., the T1D patient:

$$\begin{aligned} x_{k+1} &= f(x_k, u_k, r_k), \\ y_k &= h(x_k), \end{aligned} \tag{1}$$

where $x_k \in \mathbb{R}^{n_x}$ is the state vector, $u_k \in \mathbb{R}^{n_u}$ is the control input, and $y_k \in \mathbb{R}^{n_y}$ is the measured output. The state transition map $f(\cdot)$ and the measurement map $h(\cdot)$ are not exactly known in structure or parameters. Moreover, $r_k \in \mathbb{R}^{n_r}$ denotes an uncontrolled and partially known exogenous input, modeled as

$$r_k = \bar{r}_k + \delta r_k, \tag{2}$$

where $\bar{r}_k$ is known and $\delta r_k \in \mathbb{R}^{n_r}$ is unknown but bounded.

In this work, $x_k \in \mathbb{R}^5$ has components: $x_1$ [mg/dL], blood glucose concentration; $x_2$ [U/min], plasma insulin delivery rate; $x_3$ [U/min], subcutaneous insulin delivery rate; $x_4$ [g/min], gut glucose appearance rate; and $x_5$ [g/min], stomach glucose delivery rate. The output $y_k$ coincides with $x_1$, while the control input $u_k$ [U/min][1] corresponds to the insulin infusion commanded by the controller. The exogenous input $r_k$ captures the effect of meal intake on glucose dynamics, with $\bar{r}_k$ denoting the carbohydrate amount announced by the patient to the AP, and $\delta r_k$ representing the deviation between the announced and actual intake, accounting for possible under- and over-reporting.

For control purposes, we consider the linear affine approximation of system (1), adapted from Ruan et al. (2017),

$$\begin{aligned} x_{k+1} &= Ax_k + Bu_k + B_r\bar{r}_k + E + \delta f_k, \\ y_k &= Cx_k + \delta h_k, \end{aligned} \tag{3}$$

where matrices $A$, $B$, $B_r$, $E$, and $C$ define the linearized and discretized dynamics. The model parameters, their identification, and the discretization procedure follow Abuin et al. (2020) and are summarized in Appendix.

The terms $\delta f_k$ and $\delta h_k$ represent lumped modeling discrepancies affecting the state and output equations, respectively. They are defined as

$$\begin{aligned} \delta f_k &= f(x_k, u_k, r_k) - \big(Ax_k + Bu_k + B_r\bar{r}_k + E\big), \\ \delta h_k &= h(x_k) - Cx_k, \end{aligned} \tag{4}$$

where $\delta f_k$ accounts for unmodeled dynamics and the difference between the meal $r_k$ and its announced value $\bar{r}_k$, while $\delta h_k$ captures output-related mismatches.

### 2.2. State estimation via Kalman filter

To account for slowly varying or constant disturbances, an auxiliary disturbance state $d_k \in \mathbb{R}^{n_d}$ is introduced to capture steady-state biases in glucose dynamics. It enables offset-free control and improved state estimation, being modeled as

$$d_{k+1} = d_k, \tag{5}$$

and estimated for incorporation in the control framework, corresponding to the slowly varying or constant components of $\delta f_k$ and $\delta h_k$.

Defining an augmented state as $z_k = [x_k^\top \; d_k^\top]^\top \in \mathbb{R}^{n_x+n_d}$, the system dynamics can be rewritten as

$$\begin{aligned} z_{k+1} &= A_a z_k + B_a u_k + B_{ar}\bar{r}_k + E_a + G_a w_k, \\ y_k &= C_a z_k + v_k, \end{aligned} \tag{6}$$

[1] "U" denotes International Units of insulin (IU), i.e., the standard activity-based unit used in insulin pumps/pens. For reference, 1 U $\approx$ 34.7 $\mu$g $\approx$ 6 nmol of human insulin; clinical dosing is defined in IU rather than mass.

where the terms $w_k$ and $v_k$ represent residual process and measurement uncertainties, and the augmented matrices are given by

$$A_a = \begin{bmatrix} A & B_d \\ 0 & I \end{bmatrix}, \quad B_a = \begin{bmatrix} B \\ 0 \end{bmatrix}, \quad B_{ar} = \begin{bmatrix} B_r \\ 0 \end{bmatrix},$$
$$E_a = \begin{bmatrix} E \\ 0 \end{bmatrix}, \quad G_a = \begin{bmatrix} I \\ 0 \end{bmatrix}, \quad C_a = \begin{bmatrix} C & D_d \end{bmatrix},$$

with $I$ and 0 being, respectively, eye and zero matrices with appropriate dimensions.

The augmented system (6) is estimated by means of a linear Kalman filter. The process and measurement uncertainties are modeled as zero-mean, independent Gaussian random variables $w_k \sim \mathcal{N}(0, \Sigma_w)$ and $v_k \sim \mathcal{N}(0, \Sigma_v)$, with covariance matrices $\Sigma_w$ and $\Sigma_v$ selected as in Abuin et al. (2020). Moreover, the initial state $z_0$ is normally distributed with mean $\hat{z}_{0|0}$ and covariance $P_{0|0}$.

Given $\hat{z}_{k-1|k-1}$ and $P_{k-1|k-1}$, the one-step ahead Kalman filter prediction is computed as (Simon, 2006)

$$\hat{z}_{k|k-1} = A_a \hat{z}_{k-1|k-1} + B_a u_{k-1} + B_{ar} \bar{r}_{k-1} + E_a, \tag{7}$$
$$P_{k|k-1} = A_a P_{k-1|k-1} A_a^\top + G_a \Sigma_w G_a^\top. \tag{8}$$

Moreover, the arrival of measurement $y_k$ yields the update

$$L_k = P_{k|k-1} C_a^\top (C_a P_{k|k-1} C_a^\top + \Sigma_v)^{-1}, \tag{9}$$
$$\hat{z}_{k|k} = \hat{z}_{k|k-1} + L_k \big(y_k - C_a \hat{z}_{k|k-1}\big), \tag{10}$$
$$P_{k|k} = (I - L_k C_a) P_{k|k-1}. \tag{11}$$

The filter provides, at each step, the pair $\hat{z}_{k|k}$ and $P_{k|k}$, representing the minimum-variance estimate of the augmented state and its corresponding estimation error covariance.

### 2.3. Operational constraints

Safety and actuator limits are encoded as the polyhedral sets

$$\mathcal{X} = \{x \in \mathbb{R}^5 \mid H_x x \le h_x\}, \tag{12}$$
$$\mathcal{U} = \{u \in \mathbb{R} \mid H_u u \le h_u\}, \tag{13}$$

with

$$H_x = \begin{bmatrix} 1 & 0 & 0 & 0 & 0 \\ -1 & 0 & 0 & 0 & 0 \\ 0 & \theta_4 & \theta_4 & 0 & 0 \end{bmatrix}, \; H_u = \begin{bmatrix} 1 \\ -1 \end{bmatrix},$$
$$h_x = \begin{bmatrix} \mathrm{G_{hyper}} & -\mathrm{G_{hypo}} & \mathrm{IOB_{max}} \end{bmatrix}^\top, \; h_u = \begin{bmatrix} \mathrm{U_{max}} & 0 \end{bmatrix}^\top.$$

The parameters $\mathrm{G_{hypo}}$ and $\mathrm{G_{hyper}}$ specify the admissible range for $x_1$, defining the hypo- and hyperglycemia thresholds, respectively. The upper bound on insulin on board (IOB), which limits the residual insulin in the body from previous bolus deliveries, is defined as (Abuin et al., 2020)

$$\mathrm{IOB_{max}} = 2U_b\theta_4 + (\mathrm{CHO_{ub}}/CR) + \tau U_b,$$

where $\theta_4$ is a model parameter describing the insulin absorption dynamics (see Appendix); $U_b$ denotes the basal infusion required to maintain euglycemia under fasting conditions; $CR$ is the carbohydrate-to-insulin ratio characterizing the patient-specific relationship between ingested carbohydrates and the amount of insulin needed for their disposal; $\tau$ defines the admissible duration of basal suspension during postprandial compensation (i.e., under superbolus infusion mode); and $\mathrm{CHO_{ub}}$ represents the maximum expected carbohydrate intake, used to relax the IOB constraint during meal scenarios. It is worth highlighting that the state set is left unbounded in $x_4$ and $x_5$, reflecting their role as uncontrollable, meal-related states.

### 2.4. Uncertainty bounds

To derive the constraint tightening in the tube-based MPC formulation, a deterministic bound on the stochastic variables associated with the Kalman filter is required. These variables capture the effects of process and measurement noise and are enclosed within compact sets that hold with a prescribed probability level, constructed as uniformly bounded confidence sets (UBCS) following Joa et al. (2023). Therefore, the UBCS converts the probabilistic description of the uncertainties into a deterministic set used in the tube-based formulation to ensure constraint satisfaction with the desired confidence level.

Let $\zeta_k \sim \mathcal{N}(0, \Sigma_k)$ denote a zero-mean random variable with covariance $\Sigma_k \succeq 0$, and let $\Sigma$ be a uniform upper bound such that $\Sigma_k \preceq \Sigma$ for all $k \ge 0$. A UBCS of probability level $1 - p$ for $\zeta_k$ is defined as the smallest compact convex set satisfying

$$\mathbb{P}(\zeta_k \in \mathcal{E}^{\zeta}_{1-p}) \ge 1 - p, \quad \forall k \ge 0, \tag{14}$$

with $\mathbb{P}(\mathcal{A})$ being the probability of event $\mathcal{A}$ and $p \in (0, 1)$.

Such a set can be expressed in polyhedral form as

$$\mathcal{E}^{\zeta}_{1-p} = \{\, \zeta \in \mathbb{R}^{n_\zeta} : H_\zeta \, \zeta \le h_\zeta \,\}, \tag{15}$$

where $H_\zeta \in \mathbb{R}^{2n_\zeta \times n_\zeta}$ and $h_\zeta \in \mathbb{R}^{2n_\zeta}$ define the half-space representation of the set.

Using the eigenvector decomposition of $\Sigma = VDV^\top$, the facet normals are aligned with the covariance principal directions by setting $H_\zeta = [V \;\; -V]^\top$, yielding a origin-centered symmetric polyhedron. The offsets are defined componentwise as

$$[h_\zeta]_m = \Phi^{-1}(1 - p_m) \sqrt{[H_\zeta]_m \, \Sigma \, [H_\zeta]_m^\top}, \quad m = 1, \ldots, 2n_\zeta,$$

with $\sum_{m=1}^{2n_\zeta} p_m = p$ and $p_m \in (0, 1)$. Moreover, $\Phi(\cdot)$ denotes the cumulative distribution function of the standard normal distribution, and, considering symmetric facets and no directional preference, it can be used $p_m = p/(2n_\zeta)$.

We associate polyhedral UBCS to bound the estimator disturbances, with the confidence level $p$ acting as a tuning parameter that controls the size of the resulting deterministic uncertainty sets. Smaller values of $p$ produce larger sets that enforce stronger robustness at the expense of increased conservatism in subsequent constraint tightening procedures, whereas larger values of $p$ yield smaller sets with reduced robustness guarantees. In this work, we select $p = 0.05$, which corresponds approximately to a two-sigma confidence region for Gaussian disturbances. Thus, using the covariances $\Sigma_w$ and $\Sigma_v$, we define

$$\mathcal{E}^{w}_{1-p} = \{\, w : H_w w \le h_w \,\} \text{ and } \mathcal{E}^{v}_{1-p} = \{\, v : H_v v \le h_v \,\}.$$

## 3. Tube-based ZMPC approach

We adopt a tube framework to achieve robust constraint satisfaction under bounded process and measurement uncertainties. The implemented law is composed of a nominal law and an ancillary feedback, and we bound two coupled errors: (i) the deviation between true and nominal trajectories (mismatch error) and (ii) the deviation between true and estimated states (estimation error). Adapting the framework proposed in Joa et al. (2023), robust positive invariance of these error dynamics yields time-invariant tightenings for state and input constraints. To achieve steady-state accuracy under patient–model mismatch or constant/slow disturbances, we incorporate offset-free ingredients into the controller (Dong & Angeli, 2020). The nominal optimal control problem coincides with the ZMPC formulation of Abuin et al. (2020), with the only modifications being the replacement of the admissible state and input sets by their tube-tightened counterparts and the inclusion of relaxed lower bounds constraints to preserve feasibility. For notational simplicity, in the following we omit conditioning indices, e.g., $\hat{z}_k \equiv \hat{z}_{k|k}$.

### 3.1. Error dynamics and dual control law

To enable constraint tightening in the tube framework with estimation uncertainty, we define the estimation and mismatch errors, $\hat{e}_k$ and $\bar{e}_k$, and derive their dynamics under the dual control law $u_k$ (Joa et al., 2023). Therefore, consider the following definitions:

$$\hat{e}_k = z_k - \hat{z}_k, \tag{16}$$

$$\bar{e}_k = \hat{z}_k - \bar{z}_k, \tag{17}$$

$$u_k = \bar{u}_k + K(\hat{z}_k - \bar{z}_k), \tag{18}$$

where $K$ is chosen so that $A_K = A_a + B_aK$ is Schur and with $\bar{z}_k$ and $\bar{u}_k$ denoting the nominal augmented state and control input, respectively.

Combining (7) and (10), the one-step observer recursion can be written as

$$\hat{z}_{k+1} = A_a\hat{z}_k + B_a u_k + B_{ar}\,\bar{r}_k + E_a + L_k(y_k - C_a\hat{z}_k). \tag{19}$$

Moreover, the nominal dynamics can be obtained from (6) as

$$\bar{z}_{k+1} = A_a\bar{z}_k + B_a\bar{u}_k + B_{ar}\bar{r}_k + E_a. \tag{20}$$

Therefore, the estimation error dynamics can be obtained subtracting (19) from (6), yielding

$$\hat{e}_{k+1} = A_L\hat{e}_k + \hat{\delta}_k, \tag{21}$$

with $A_L = A_a - L_kC_a$ and $\hat{\delta}_k = G_a w_k - L_k v_k$. Likewise, from Eqs. (17) to (20), the mismatch error dynamics results

$$\bar{e}_{k+1} = A_K\bar{e}_k + \bar{\delta}_k, \tag{22}$$

with $\bar{\delta}_k = L_k(C_a\hat{e}_k + v_k)$.

**Remark 1.** Because of the disturbance augmentation and additional uncontrollable states, a gain matrix $K$ rendering $A_a + B_aK$ Schur on the whole space may not exist. In such cases, we design $K_c$ on the controllable subspace so that the controllable portion of the system is Schur, and we use the block-augmented gain $K = [K_c\ 0]$ in the dual law.

### 3.2. Robust invariant sets and constraint tightening

Following the procedure proposed in Joa et al. (2023), it is possible to obtain a bound $P_k \preceq P_{\mathrm{MD}}$ defined as

$$P_{\mathrm{MD}} = A_a^{-1}(P_\infty - \Sigma_w)(A_a^\top)^{-1}, \tag{23}$$

where $P_\infty$ is obtained by solving the Riccati equation $P_\infty = A_a(P_\infty - P_\infty C_a^\top(C_aP_\infty C_a^\top + \Sigma_v)^{-1}C_aP_\infty)A_a^\top + \Sigma_w$. Applying the Kalman gain expression (9) to this covariance upper bound yields the constant gain

$$L_{\mathrm{MD}} = P_{\mathrm{MD}}C_a^\top(C_aP_{\mathrm{MD}}C_a^\top + \Sigma_v)^{-1}. \tag{24}$$

Considering the estimation error dynamics and $L_{\mathrm{MD}}$, the disturbance set can be defined as

$$\hat{\Delta} = G_a\mathcal{E}^w_{1-p} \oplus (-L_{\mathrm{MD}})\mathcal{E}^v_{1-p}, \tag{25}$$

such that $\hat{\delta}_k \in \hat{\Delta}$ for all $k \geq 0$ and with $\oplus$ denoting the Minkowski sum operator.

A robust positively invariant (RPI) set $\hat{\mathcal{S}}$ for $\hat{e}$ must satisfies

$$A_L\hat{\mathcal{S}} \oplus \hat{\Delta} \subseteq \hat{\mathcal{S}}. \tag{26}$$

Similarly, an RPI set $\bar{\mathcal{S}}$ for $\bar{e}$ must satisfies

$$A_K\bar{\mathcal{S}} \oplus \bar{\Delta} \subseteq \bar{\mathcal{S}}, \tag{27}$$

with $\bar{\Delta} = L_{\mathrm{MD}}\big(C_a\hat{\mathcal{S}} \oplus \mathcal{E}^v_{1-p}\big)$, such that $\bar{\delta}_k \in \bar{\Delta}$ for all $k \geq 0$. These conditions characterize the class of sets that guarantee invariance of the estimation and mismatch error dynamics under bounded disturbances.

To construct such invariant sets in a systematic and minimally conservative manner, consider a linear map $F$ and disturbance set $\mathcal{W}$. A minimal outer RPI set $\Omega$ can be computed based on the recursion

$$\Omega_0 = \{0\}, \qquad \Omega_{i+1} = F\,\Omega_i \oplus \mathcal{W}. \tag{28}$$

In practice, for the monotone sequence $\Omega_i \subseteq \Omega_{i+1}$, the recursion stops at the first index $j$ such that $\Omega_{j+1} \subseteq \Omega_j$. The resulting set $\Omega_\infty = \Omega_j$ is the minimal outer RPI set (Kerrigan, 2000). This procedure is used here to compute invariant bounds for the estimation and mismatch error dynamics by selecting $F$ and $\mathcal{W}$ according to the corresponding dynamics and disturbance sets, thereby supporting the construction of the sets $\hat{\mathcal{S}}$ and $\bar{\mathcal{S}}$.

From (16) and (17), the augmented state can be decomposed as

$$z_k = \bar{z}_k + \bar{e}_k + \hat{e}_k. \tag{29}$$

Thus, if $z_k \in \mathcal{Z}$, this is enforced on the nominal component as

$$\bar{z}_k \in \mathcal{Z} \ominus (\bar{\mathcal{S}} \oplus \hat{\mathcal{S}}), \tag{30}$$

with $\ominus$ denoting the Pontryagin difference.

Then, $x_k \in \mathcal{X}$ for all $\bar{e}_k \in \bar{\mathcal{S}}$ and $\hat{e}_k \in \hat{\mathcal{S}}$ can be imposed as

$$\bar{x}_k \in \bar{\mathcal{X}}, \tag{31}$$

where $\bar{\mathcal{X}} = \mathcal{X} \ominus \mathrm{Proj}_{\mathcal{X}}(\bar{\mathcal{S}} \oplus \hat{\mathcal{S}})$ with $\bar{x}_k$ being the nominal component of the state vector and $\mathrm{Proj}_{\mathcal{X}}(\cdot)$ denoting the projection of $(\cdot)$ onto the state space $\mathcal{X}$.

Likewise, since $u_k = \bar{u}_k + K\,\bar{e}_k$, for all $\bar{e}_k \in \bar{\mathcal{S}}$ the constraint $u_k \in \mathcal{U}$ is ensured by

$$\bar{u}_k \in \bar{\mathcal{U}}, \tag{32}$$

with $\bar{\mathcal{U}} = \mathcal{U} \ominus K\bar{\mathcal{S}}$.

### 3.3. Nominal ZMPC

For a prediction horizon $N \in \mathbb{N}$, at each sampling instant $k$ the nominal ZMPC computes the input sequence $\bar{\boldsymbol{u}} = \{\bar{u}_0, \bar{u}_1, \ldots, \bar{u}_{N-1}\}$ that steers the output toward the target zone $\mathcal{Y}^{\mathrm{Tar}} \in [\mathcal{Y}^{\mathrm{tar}}_{\min}, \mathcal{Y}^{\mathrm{tar}}_{\max}]$ while satisfying the operational constraints. The optimization is carried out in a receding-horizon fashion, where the Kalman filter provides the current state estimate $\hat{x}_k$ used to initialize the predictions. After solving the problem, only the first element of the optimal sequence $\bar{u}_0$ is applied, and the procedure is repeated at the next sampling instant. Moreover, following Abuin et al. (2020), the announced meal $\bar{r}_k$ is treated as an exogenous input profile incorporated into the prediction model to capture the anticipated impact of meal intake within the prediction horizon. The cost function to be minimized by the MPC controller is given by

$$V_N(\hat{x}_k, \bar{r}_k, \mathcal{Y}^{\mathrm{Tar}}; \bar{\boldsymbol{u}}, \bar{u}_a, \bar{y}_a, \delta_{\mathrm{hyper}}, \delta_{\mathrm{hypo}}) = V^d_N(\hat{x}_k, \bar{r}_k; \bar{\boldsymbol{u}}, \bar{u}_a, \bar{y}_a) + V^s_N(\mathcal{Y}^{\mathrm{Tar}}; \delta_{\mathrm{hyper}}, \delta_{\mathrm{hypo}}), \tag{33}$$

where

$$V^d_N(\hat{x}_k, \bar{r}_k; \bar{\boldsymbol{u}}, \bar{u}_a, \bar{y}_a) = \sum_{j=0}^{N-1} \|C\bar{x}_j - \bar{y}_a\|^2_Q + \|\bar{u}_j - \bar{u}_a\|^2_R,$$

$$V^s_N(\mathcal{Y}^{\mathrm{Tar}}; \delta_{\mathrm{hyper}}, \delta_{\mathrm{hypo}}) = \hat{\rho}\delta^2_{\mathrm{hyper}} + \check{\rho}\delta^2_{\mathrm{hypo}},$$

are, respectively, dynamic and stationary costs.

The dynamic cost $V^d_N(\cdot)$ steers the predicted trajectories toward the artificial steady variables $(u_a, y_a)$ through the weighting matrices $Q \succeq 0$ and $R \succ 0$, whereas the stationary term $V^s_N(\cdot)$ penalizes deviations of $y_a$ from the target zone $\mathcal{Y}^{\mathrm{Tar}}$. The

nonnegative slack variables $\delta_{\text{hypo}}$ and $\delta_{\text{hyper}}$ represent penalties associated with hypoglycemia and hyperglycemia, respectively, and are weighted by $\check{\rho}$ and $\hat{\rho}$, chosen such that $\hat{\rho} \ll \check{\rho}$ to impose a stronger penalty on hypoglycemia and thus ensure asymmetric protection in the lower bound of the zone.

The nominal optimal control problem solved by the ZMPC at time $k$ over the prediction horizon $N$ is given by

$$\min_{\substack{\bar{\boldsymbol{u}},\bar{u}_a,\bar{x}_a,\bar{y}_a,\\ \delta_{\text{hyper}},\delta_{\text{hypo}}}} \quad V_N(\hat{x}_k, \bar{r}_k, \mathcal{Y}^{\text{Tar}}; \bar{\boldsymbol{u}}, \bar{u}_a, \bar{y}_a, \delta_{\text{hyper}}, \delta_{\text{hypo}})$$

$$\text{s.t.} \quad \bar{x}_0 = \hat{x}_k, \tag{34a}$$

$$\bar{x}_{j+1} = A\bar{x}_j + B\bar{u}_j + B_r\bar{r}_j + E, \quad j \in \mathbb{I}_{0:N-1}, \tag{34b}$$

$$\bar{y}_j = C\bar{x}_j, \quad j \in \mathbb{I}_{0:N-1}, \tag{34c}$$

$$\bar{u}_j \in \bar{\mathcal{U}}, \quad j \in \mathbb{I}_{0:N-1}, \tag{34d}$$

$$\bar{x}_j \in \bar{\mathcal{X}}, \quad j \in \mathbb{I}_{0:N-1}, \tag{34e}$$

$$\bar{x}_a = A\bar{x}_a + B\bar{u}_a + E, \tag{34f}$$

$$\bar{y}_a = C\bar{x}_a, \tag{34g}$$

$$(\bar{x}_a, \bar{u}_a) \in \bar{\mathcal{X}} \times \bar{\mathcal{U}}, \tag{34h}$$

$$\bar{x}_N = x_a, \tag{34i}$$

$$y_a \in [\mathcal{Y}^{\text{tar}}_{\min} - \delta_{\text{hypo}},\ \mathcal{Y}^{\text{tar}}_{\max} + \delta_{\text{hyper}}], \tag{34j}$$

$$\delta_{\text{hypo}} \geq 0,\ \delta_{\text{hyper}} \geq 0. \tag{34k}$$

In the problem ((34)), the prediction model (34b)–(34c) propagates the nominal trajectories over the horizon $N$ starting from the estimate $\hat{x}_k$ as imposed by (34a). Constraints (34d)–(34e) enforce tightened input and state limits, ensuring that all predicted variables remain within the feasible region under uncertainty. Constraints (34f)–(34h) define a feasible artificial steady triplet $(\bar{x}_a, \bar{u}_a, \bar{y}_a)$ consistent with the nominal model and disregarding the exogenous input $\bar{r}$, while (34i) imposes a relaxed terminal equality condition. Finally, the zone constraint (34j) ensures that $\bar{y}_a$ remains within the desired target region.

### 3.4. Soft lower bounds for nonnegative inputs

The considered system belongs to the class of nonnegative systems, as physiological variables are inherently nonnegative. In tube-based MPC, standard tightening may exclude admissible near-origin equilibria, resulting in the infeasibility of the nominal problem. To the best of the authors' knowledge, the design of tightening schemes that preserve such equilibria in positive systems remains an open problem. To address this without compromising robustness, the lower bounds of the insulin and IOB constraints are softly relaxed, while all upper bounds remain as defined by the tightened procedure. From a robustness standpoint, this relaxation is justified since reducing insulin delivery or IOB does not compromise safety and corresponds to a cautious approach to preserve constraint satisfaction under uncertainty, whereas violating upper bounds (i.e., delivering too much insulin) would be unsafe.

Let $s_x(j)$ and $s_u(j)$ be nonnegative slack variables introduced at each stage $j \in \mathbb{I}_{0:N-1}$ as additional decision variables to relax selected lower bounds, defined as

$$\bar{H}_x\bar{x}_j \leq \bar{h}_x + S_x s_x(j), \quad \bar{H}_u\bar{u}_j \leq \bar{h}_u + S_u s_u(j),$$

where $S_x$ and $S_u$ are selection matrices activating only the bounds to be softened and with $\bar{H}_x$, $\bar{h}_x$, $\bar{H}_u$, and $\bar{h}_u$ defining the tightened sets $\bar{\mathcal{X}} = \{\bar{H}_x\bar{x} \leq \bar{h}_x\}$ and $\bar{\mathcal{U}} = \{\bar{H}_u\bar{u} \leq \bar{h}_u\}$. Moreover, through the weights $\Lambda_x$, $\Lambda_u \succ 0$, the cost function is augmented to penalize constraint violations, given by $V_N^{\text{a}}(\cdot) = V_N(\cdot) + \sum_{j=0}^{N-1} \|s_x(j)\|^2_{\Lambda_x} + \|s_u(j)\|^2_{\Lambda_u}$.

## 4. Scenario and parameters

The efficacy of the proposed robust ZMPC was assessed through *in silico* experiments on a cohort of 10 adult virtual subjects from the FDA-approved UVA/Padova metabolic simulator (The Epsilon Group, 2016). For a fair comparison, the otherwise identical nominal ZMPC proposed by Abuin et al. (2020) was evaluated in parallel. In particular, the baseline controller is nominal and does not explicitly account for uncertainty (hence it does not apply tube-based constraint tightening), whereas the proposed method explicitly propagates bounded uncertainty through a tube to enforce tightened safety constraints. Each subject was simulated continuously for 7 days. Controllers were implemented in MATLAB with the CasADi framework (Andersson et al., 2019).

### 4.1. Scenario setup

To stress-test robustness, we exposed both controllers to multiple, concurrent uncertainty sources: (i) Model–plant mismatch induced by using a linear physiological prediction model to control the nonlinear simulator, (ii) Added intraday physiological variability in insulin sensitivity following the proposal in Toffanin et al. (2013), and (iii) Misannounced meal disturbances, i.e. for every meal event, the carbohydrate amount communicated to the controller was randomly either overestimated by 50% or underestimated by 50% relative to the true intake.

The daily meal plan comprised three nominal meals: 60 g at 07:00, 60 g at 12:00, and 80 g at 18:00, with respective durations of 30, 30, and 40 min. To reflect more realistic eating behavior, the standard meal plan was subjected to random variations in the meal start time ($\pm$10 minutes), carbohydrate content ($\pm$20%), and duration ($\pm$10 minutes). The misannouncement mechanism operated on these meals as described above, thereby creating a substantial and realistic mismatch between the announced and actual disturbances.

The simulation environment emulated standard clinical hardware. Glucose sensing was modeled after the Dexcom G5 Mobile CGM (Vettoretti et al., 2018), and insulin delivery used a default pump model with a maximum infusion rate of $U_{\max} = 15$ U/min (MiniMed, 2018). Insulin was delivered in 1-minute pulses (Abuin et al., 2020), while the MPC sampling time was $T_s = 5$ min.

### 4.2. MPC setup and performance metrics

Both the robust and the nominal controllers shared the same MPC settings to isolate the effect of robustness. Specifically, the quadratic stage cost was setted with weights $Q = 1$ and $R = 100$, and an asymmetric terminal cost targeted a glycemic zone in which hypoglycemia was penalized more heavily than hyperglycemia (i.e., $\hat{\rho} = 10^6$ for hyperglycemia and $\check{\rho} = 10^9$ for hypoglycemia). Weights $\Lambda_x = \Lambda_u = 10$ have been chosen, in such a way that the control can easily fall below the lower tightened bound maintaining the safety of the application, as detailed in Section 3.4. A prediction horizon of 6 h ($N = 72$ steps) was adopted, consistent with clinical guidance (American Diabetes Association, 2018). Safety constraints bounded the predicted glucose trajectory between $G_{\text{hypo}} = 60$ mg/dL and $G_{\text{hyper}} = 300$ mg/dL, and a terminal constraint guided predictions toward the normoglycemic target range $\mathcal{Y}^{\text{tar}}_{\min} = 90$ - $\mathcal{Y}^{\text{tar}}_{\max} = 120$ mg/dL. The upper bound on IOB was limited considering the parameters $\tau = 90$ min, $\text{CHO}_{\text{ub}} = 120$ g, $U_b = (\theta_0 - \theta_1 \cdot G_{\text{hypo}})/\theta_2$, $\theta_4$, $CR = \theta_2/\theta_3$, as reported in Abuin et al. (2020).

Controller performance was quantified using standard CGM-based metrics, summarized across subjects by the median [25th,

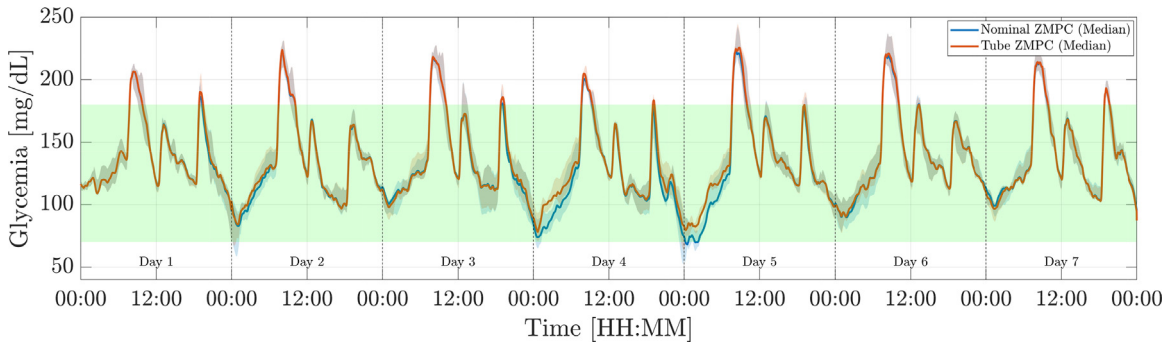


**Fig. 1.** Comparative glycemic profiles for the Nominal ZMPC (blue) and the Tube ZMPC (red) over a 7-day in silico simulation period. The solid lines represent the median glucose trajectory across the cohort of 10 virtual subjects, while the shaded areas depict the interquartile range (25th to 75th percentile), illustrating inter-subject variability. The horizontal green band indicates the target euglycemic range (70–180 mg/dL). The figure highlights the Tube ZMPC's more conservative action in preventing excursions below the target range.

**Table 1**
Comparison of glycemic metrics for nominal and tube ZMPC controllers.

| Metric | Nominal ZMPC | Tube ZMPC |
|---|---|---|
| $\bar{G}_m$ [mg/dL] | 132.7 [132.0–136.5] | 134.7 [133.3–138.6] |
| SD [mg/dL] | 35.3 [31.3–38.3] | 34.3 [30.7–36.9] |
| CV [%] | 27.4 [23.2–28.4] | 26.0 [22.7–27.5] |
| $T_{70-140}$ [%] | 64.7 [60.3–65.5] | 65.7 [60.4–66.4] |
| $T_{70-180}$ [%] | 86.1 [84.4–89.8] | 87.9 [84.8–90.3] |
| $T_{>180}$[%] | 11.6 [9.2–14.3] | 12.1 [9.3–14.5] |
| $T_{>250}$ [%] | 0.0 [0.0–0.0] | 0.0 [0.0–0.0] |
| $T_{<70}$ [%] | 1.6 [0.5–2.3] | 0.0 [0.0–0.9] |
| $T_{<54}$ [%] | 0.1 [0.0–0.3] | 0.0 [0.0–0.0] |
| TDI [U] | 44.9 [42.7–55.5] | 44.8 [42.5–55.4] |

75th percentile]. The indices included mean glucose ($\bar{G}_m$), standard deviation (SD), coefficient of variation (CV), and the percentages of time in euglycemia ($T_{70-180}$), tight euglycemia ($T_{70-140}$), hyperglycemia ($T_{>180}$, $T_{>250}$), and hypoglycemia ($T_{<70}$, $T_{<54}$), where $T_{>250}$, and $T_{<54}$ denotes the percentage of time with glucose in severe condition, hence above 250 mg/dL (severe hyperglycemia), and below 54 mg/dL (severe hypoglycemia). Total daily insulin (TDI) was also recorded. Overall glycemic control patterns were visualized via Control Variability Grid Analysis (CVGA) (Magni et al., 2008), providing a compact overview of cohort-level outcomes.

## 5. Results and discussion

The efficacy of the proposed robust ZMPC (Tube ZMPC) was benchmarked against an identical nominal ZMPC controller through a series of *in silico* experiments. The comparative glycemic performance metrics, aggregated across the cohort of 10 virtual adult subjects, are detailed in Table 1.

Overall, both controllers maintained commendable glycemic control despite the persistent disturbances. The median Time in Range and Time in Tight Range were high and closely matched for both the Nominal ZMPC (86.1% and 64.7%) and the Tube ZMPC (87.9% and 65.7%). Variability was slightly lower with the robust controller (SD 34.3 [30.7–36.9] mg/dL and CV 26.0% [22.7–27.5]) compared with the nominal controller (SD 35.3 [31.3–38.3] mg/dL and CV 27.4% [23.2–28.4]). Both strategies delivered essentially the same median Total Daily Insulin (TDI), 44.9 [42.7–55.5] U for Nominal vs. 44.8 [42.5–55.4] U for Tube, suggesting that the enhanced safety of the robust controller did not come at the cost of increased insulin consumption.

The clearest difference appears in hypoglycemia avoidance. The Tube ZMPC reduced median Time Below Range to 0.0% [0.0–0.9], compared with 1.6% [0.5–2.3] for the Nominal ZMPC, reflecting both a lower central tendency and a tighter upper spread. Severe hypoglycemia was eliminated by the robust controller with $T_{<54} = 0.0\%$ [0.0–0.0] across the cohort, whereas the nominal controller showed a small but nonzero median of 0.1% [0.0–0.3]. These findings indicate a meaningful improvement in safety under Tube ZMPC without sacrificing overall control or insulin usage. In terms of hyperglycemia, performance remained closely matched. The Tube ZMPC exhibited a slightly higher mean glucose (134.7 vs. 132.7 mg/dL) and a marginally higher $T_{>180}$ (12.1% vs. 11.6%). This is a predictable trade-off for its more cautious insulin dosing strategy in the face of uncertainty, which prioritizes the prevention of dangerous hypoglycemic events. Both controllers effectively prevented severe hyperglycemia, with $T_{>250} = 0.0\%$ for the entire cohort. The comparative glycemic profiles are visualized in Fig. 1, which illustrates the median glucose trajectories and inter-subject variability for both controllers in the overall simulation. The plot visually confirms the tight regulation of both strategies but highlights the Tube ZMPC's reduced excursions into the hypoglycemic range. The cohort-level CVGA in Fig. 2 places most outcomes within clinically acceptable regions, with several Tube ZMPC points shifting toward improved zones relative to their nominal counterparts and no worsening into unsafe regions. Taken together, the Tube ZMPC improves hypoglycemia safety and slightly reduces variability while preserving overall glycemic control and insulin requirements.

Lastly, Fig. 3 illustrates the insulin control action $u$ under the proposed tube-based ZMPC. The three peaks correspond to meal-related bolus deliveries (e.g., breakfast, lunch, and dinner), whereas between meals the controller approaches basal infusion, which can be close to zero under the adopted pulsatile delivery scheme. The dashed horizontal lines denote the tube-induced tightened input bounds; due to this tightening, the effective lower bound becomes strictly positive, incorrectly implying $u$ must always remain above zero. As discussed in Section 3.4, we therefore introduced a soft lower bound on insulin (and IOB), permitting temporary, penalized violations. This relaxation preserves feasibility for a nonnegative physiological system and maintains robustness without compromising safety.

## 6. Conclusion

We presented a robust ZMPC strategy for AP systems that translates estimator uncertainty into safety margins through tube-based constraint tightening. Using offset-free Kalman filtering, covariance information is converted into uniformly bounded confidence sets that inform constraint tightenings on glucose and insulin trajectories. Practical feasibility is maintained via softened lower bounds on insulin infusion and IOB, enabling physiologically consistent behavior without undue conservatism. The resulting controller is compatible with existing MPC implementations and preserves computational tractability.

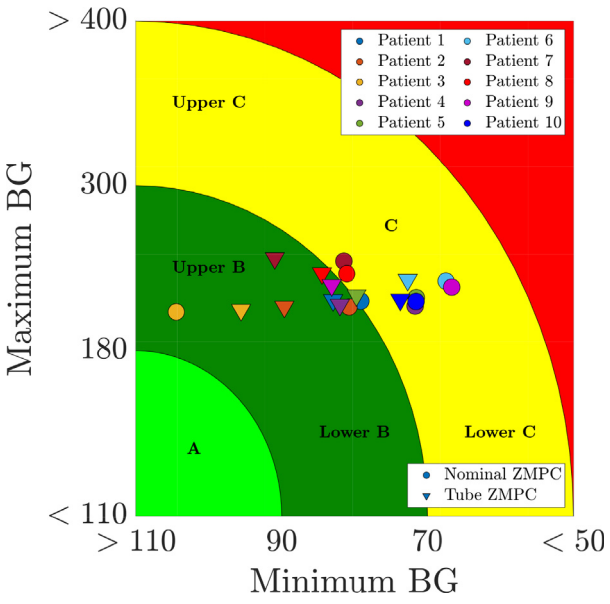


**Fig. 2.** CVGA plot comparing the performance of the Nominal ZMPC (circles) and Tube ZMPC (triangles). Each point represents the glycemic excursion (minimum vs. maximum glucose values) for a single subject over the 7-day simulation. The grid is divided into zones reflecting control quality, from accurate control (Zones A, B) to significant risk of hypoglycemia (Zones C, D, E). The plot demonstrates a critical improvement with the Tube ZMPC, which successfully shifts most of the subjects from the risky C zone into the clinically acceptable B zone, indicating a marked enhancement in safety and reduction in hypoglycemic events.

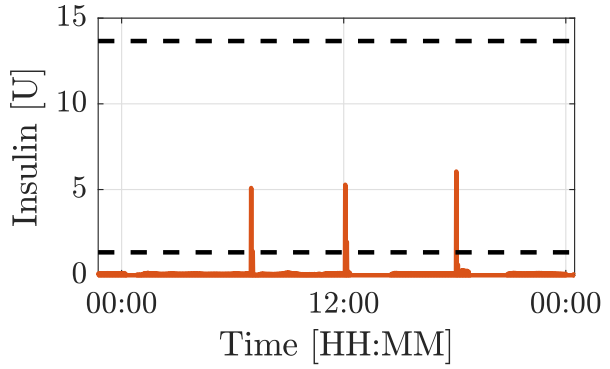


**Fig. 3.** Control input (insulin) with tube-based constraint tightening (dashed bounds). Because the tightened lower bound can become positive, a soft lower bound is adopted so $u(k)$ can drop below the tightened limit while penalized, as discussed in Section 3.4.

In silico evaluation with the FDA-accepted UVA/Padova Type 1 Diabetes simulator showed meaningful safety improvements over a nominal ZMPC baseline; notably, hypoglycemia was reduced, and severe hypoglycemia was eliminated across the cohort, reflecting a lower violation risk without increasing total daily insulin. A slight trade-off was observed in mean glucose and time above range, consistent with the controller's cautious dosing under uncertainty. Overall, the results demonstrate that incorporating estimator uncertainty into constraint management enhances robustness and hypoglycemia protection while maintaining effective glycemic control. The proposed framework offers a principled, practical route toward safer autonomous insulin delivery within existing artificial pancreas systems.

Future works will extend the framework toward adaptive tube formulations that explicitly exploit meal-related uncertainty information, using worst-case bounds or homothetic principles to adjust the tube geometry in real time. Moreover, we will investigate tube-based MPC theory for nonnegative systems to ensure feasibility near the origin without relying on soft relaxations.

## CRediT authorship contribution statement

**Nicola Licini:** Writing – review & editing, Writing – original draft, Validation, Software, Investigation, Formal analysis, Conceptualization. **Marcelo Alves Santos:** Writing – review & editing, Writing – original draft, Supervision, Investigation, Formal analysis, Conceptualization. **Fabio Previdi:** Supervision, Funding acquisition. **Antonio Ferramosca:** Supervision, Formal analysis, Conceptualization.

## Declaration of competing interest

The authors declare that they have no known competing financial interests or personal relationships that could have appeared to influence the work reported in this paper.

## Appendix. Control-oriented model

In this work the glucose–insulin we consider the glucose–insulin regulation problem under exogenous inputs, i.e., meal announcements, and measurement noise. The model adopted in this work follows the proposal by Ruan et al. (2017), described as follows

$$\begin{aligned} \dot{x}(t) &= A^c x(t) + B_u^c u(t) + B_r^c r(t) + E^c, \\ y(t) &= Cx(t), \end{aligned} \tag{A.1}$$

where the state vector $x(t) \in \mathbb{R}^{5\times 1}$, is defined as $x(t) = [x_1(t), x_2(t), x_3(t), x_4(t), x_5(t)]^T$, where $x_1$ [mg/dL] is the blood glucose concentration, i.e. the output $y(t)$ to be controlled, $x_2$ [U/min] is the insulin delivery rate in plasma, $x_3$ [U/min] is the insulin delivery rate in the subcutaneous compartment, $x_4$ [g/min] is the glucose absorption rate from the gut, and $x_5$ [g/min] is the glucose delivery rate from the stomach. The inputs are $u(t)$, i.e., the insulin infusion rate [U/min], and $r(t)$, i.e., the rate of carbohydrate intake [g/min]. The continuous state and input matrix are defined as:

$$A^c = \begin{bmatrix} -\theta_1 & -\theta_2 & 0 & \theta_3 & 0 \\ 0 & -\frac{1}{\theta_4} & \frac{1}{\theta_4} & 0 & 0 \\ 0 & 0 & -\frac{1}{\theta_4} & 0 & 0 \\ 0 & 0 & 0 & -\frac{1}{\theta_5} & \frac{1}{\theta_5} \\ 0 & 0 & 0 & 0 & -\frac{1}{\theta_5} \end{bmatrix},$$

$$B_u^c = \begin{bmatrix} 0 \\ 0 \\ \frac{1}{\theta_4} \\ 0 \\ 0 \end{bmatrix}, \quad B_r^c = \begin{bmatrix} 0 \\ 0 \\ 0 \\ 0 \\ \frac{1}{\theta_5} \end{bmatrix}, \quad E^c = \begin{bmatrix} \theta_0 \\ 0 \\ 0 \\ 0 \\ 0 \end{bmatrix}, C = \begin{bmatrix} 1 \\ 0 \\ 0 \\ 0 \\ 0 \end{bmatrix}^\top.$$

The parameters describing glucose–insulin dynamics are detailed in Table A.1.

Discretization. To utilize the continuous-time model (A.1) effectively within an MPC controller, it has first been discretized following the approach proposed in Abuin et al. (2020): a standard zero-order hold assumption is slightly modified to a pulsatile input scheme, in order to deal with short-duration insulin actions, which are safer for the subject and provide an improved control strategy (Song et al., 2000). The resulting discrete-time model, with $A$, $B_u$, $B_r$, and $E$ denoting the discretized counterparts of $A^c$, $B_u^c$, $B_r^c$, and $E^c$, respectively, corresponds to the formulation reported in (3) and is used for prediction and control within this work.

**Table A.1**
Model parameters description.

| Parameter | Description |
|---|---|
| $\theta_0$ [mg/(dL min)] | Endogenous glucose production (EGP) |
| $\theta_1$ [1/min] | Glucose effectiveness |
| $\theta_2$ [mg/(dL U)] | Insulin sensitivity |
| $\theta_3$ [mg/(dL g)] | Carbohydrate factor |
| $\theta_4$ [min] | Insulin absorption time constant |
| $\theta_5$ [min] | Meals absorption time constant |

## References


Abuin, P., Rivadeneira, P., Ferramosca, A., & González, A. (2020). Artificial pancreas under stable pulsatile MPC: improving the closed-loop performance. *Journal of Process Control*, *92*, 246–260.

American Diabetes Association (2018). 6. glycemic targets: standards of medical care in diabetes—2019. *Diabetes Care*, *42*(Supplement_1), S61–S70.

Andersson, J. A. E., Gillis, J., Horn, G., Rawlings, J. B., & Diehl, M. (2019). CasADi: A software framework for nonlinear optimization and optimal control. *Mathematical Programming Computation*, *11*(1), 1–36.

Colmegna, P., Díaz, J. L., Garcia-Tirado, J., & Breton, M. D. (2022). Enabling anticipatory response in multi-stage MPC formulation for fully automated artificial pancreas system. In *2022 IEEE 61st conference on decision and control* (pp. 2566–2571). IEEE.

Ding, Y., Wang, L., Li, Y., & Li, D. (2018). Model predictive control and its application in agriculture: A review. *Computers and Electronics in Agriculture*, *151*, 104–117.

Dong, Z., & Angeli, D. (2020). Homothetic tube-based robust offset-free economic model predictive control. *Automatica*, *119*, Article 109105.

Jia, R., Zhao, X., Zhang, S., & Yu, X. (2024). A tube-NMPC approach for robust control of glucose in type 1 diabetes mellitus. *IEEE Transactions on Automation Science and Engineering*.

Joa, E., Bujarbaruah, M., & Borrelli, F. (2023). Output feedback stochastic MPC with hard input constraints. In *2023 American control conference* (pp. 2034–2039). IEEE.

Katsarou, A., Gudbjörnsdottir, S., Rawshani, A., Dabelea, D., Bonifacio, E., Anderson, B. J., Jacobsen, L. M., Schatz, D. A., & Lernmark, A. (2017). Type 1 diabetes mellitus. *Nature Reviews Disease Primers*, *3*(1), 17016.

Kerrigan, E. C. (2000). *Robust constraint satisfaction: Invariant sets and predictive control*. University of London.

Kirchsteiger, H., & del Re, L. (2013). Robust tube-based predictive control of blood glucose concentration in type 1 diabetes. In *52nd IEEE conference on decision and control* (pp. 2084–2089). IEEE.

Magni, L., Raimondo, D. M., Bossi, L., Dalla Man, C., De Nicolao, G., Kovatchev, B., & Cobelli, C. (2007). Model predictive control of type 1 diabetes: an in silico trial.

Magni, L., Raimondo, D. M., Man, C. D., Breton, M., Patek, S., De Nicolao, G., Cobelli, C., & Kovatchev, B. P. (2008). Evaluating the efficacy of closed-loop glucose regulation via control-variability grid analysis. *Journal of Diabetes Science and Technology*, *2*(4), 630–635.

Man, C. D., Micheletto, F., Lv, D., Breton, M., Kovatchev, B., & Cobelli, C. (2014). The UVA/PADOVA Type 1 diabetes simulator: new features. *Journal of Diabetes Science and Technology*, *8*(1), 26–34.

Mayne, D. Q., Seron, M. M., & Raković, S. V. (2005). Robust model predictive control of constrained linear systems with bounded disturbances. *Automatica*, *41*(2), 219–224.

Messori, M., Paolo Incremona, G., Cobelli, C., & Magni, L. (2018). Individualized model predictive control for the artificial pancreas: in silico evaluation of closed-loop glucose control. *IEEE Control Systems*, *38*(1), 86–104.

MiniMed, M. (2018). MINIMED™ 670g SYSTEM USer GUIDE. *Medtronic MiniMed*.

Mirshams, M., & Khosrojerdi, M. (2016). Attitude control of an underactuated spacecraft using tube-based mpc approach. *Aerospace Science and Technology*, *48*, 140–145.

Reiterer, F., Freckmann, G., & del Re, L. (2018). Impact of carbohydrate counting errors on glycemic control in type 1 diabetes. *IFAC-PapersOnLine*, *51*(27), 186–191.

Ruan, Y., Wilinska, M. E., Thabit, H., & Hovorka, R. (2017). Modeling day-to-day variability of glucose–insulin regulation over 12-week home use of closed-loop insulin delivery. *IEEE Transactions on Biomedical Engineering*, *64*(6), 1412–1419.

Simon, D. (2006). *Optimal state estimation: Kalman, H infinity, and nonlinear approaches*. John Wiley & Sons.

Song, S. H., McIntyre, S. S., Shah, H., Veldhuis, J. D., Hayes, P. C., & Butler, P. C. (2000). Direct measurement of pulsatile insulin secretion from the portal vein in human subjects. *The Journal of Clinical Endocrinology & Metabolism*, *85*(12), 4491–4499.

The Epsilon Group (2016). DMMS.R. T. E. Group.

Toffanin, C., Zisser, H., Doyle, F. J., & Dassau, E. (2013). Dynamic insulin on board: incorporation of circadian insulin sensitivity variation. *Journal of Diabetes Science and Technology*, *7*(4), 928–940.

Vettoretti, M., Facchinetti, A., Sparacino, G., & Cobelli, C. (2018). Type-1 diabetes patient decision simulator for in silico testing safety and effectiveness of insulin treatments. *IEEE Transactions on Biomedical Engineering*, *65*(6), 1281–1290.